Defossilization and decarbonization of hydrogen production using plastic waste: Temperature and feedstock effects during thermolysis stage

Andrei Veksha [a,*], Yuxin Wang [a,b], Jun Wei Foo [a], Ichiro Naruse [c], Grzegoz Lisak [a,d,**]

[a] *Residues and Resource Reclamation Centre (R3C), Nanyang Environment and Water Research Institute, Nanyang Technological University, 637141, Singapore.*

[b] *Department of Mechanical Systems Engineering, Nagoya University, Tokai National Higher Education and Research, 464-8603, Japan*

[c] *Institute of Materials and Systems for Sustainability, Nagoya University, Tokai National Higher Education and Research, 464-8601, Japan*

[d] *School of Civil and Environmental Engineering, Nanyang Technological University, 50 Nanyang Avenue, 639798, Singapore.*

*Corresponding authors: A. Veksha (aveksha@ntu.edu.sg) and G. Lisak (g.lisak@ntu.edu.sg).

Abstract

The replacement of natural gas with plastic-derived pyrolysis gas can defossilize H_2 production, while subsequent capture, utilization and storage of carbon in a solid form can decarbonize the process. The objective of this study was to investigate H_2 production from three types of plastics using a process comprising pyrolysis (600 °C) and thermolysis stages (1200-1500 °C). Depending on the plastic feedstock and thermolysis temperature, the laboratory-scale setup generated 1000-1350 mL/min product gas with H_2 purity of 74.3-94.2 vol.%. The recovery of 5-9 wt.% molecular H_2 per mass of plastics was achieved. Other products included solid residue (0.1-12 wt.%) and oil (8-52 wt.%) from the pyrolysis reactor, solid carbon (36-53 wt.%) and gas impurities (2-16 wt.%) from the thermolysis reactor. The purity of H_2 gas was detrimentally influenced by polyethylene terephthalate in the feedstock due to the dilution of gas by CO. The decomposition of methane containing in the pyrolysis gas was the limiting reaction step during H_2 production and improved at higher thermolysis temperature. Three solid carbon structures were formed during the thermolysis stage regardless of the plastic type: carbon black aggregates, carbon black aggregates coated with a layer of pyrolytic carbon and a carbon film on the inner reactor wall. Among the three types of carbon, the highest valorization potential was identified for carbon black aggregates. Plastic feedstock composition had little if any effect on carbon black properties, while high thermolysis temperature (1500 °C) reduced the particle sizes and increased the surface area of aggregates.

Keywords: carbon black; hydrogen; plastic waste; pyrolysis; thermolysis.

1. Introduction

Hydrogen is considered a key resource for decarbonized economy. However, current hydrogen production relies heavily on fossil feedstock. Approx. 95-96% of hydrogen supply originates from coal gasification and natural gas (methane) steam reforming [1]. Methane is a "cleaner" fossil feedstock compared to coal. The estimated CO_2 emissions from steam methane reforming are 9-11.5 tonnes per 1 tonne of hydrogen [2], which is nearly two times lower than from coal gasification [3]. Several technologies are being developed to reduce carbon footprint of hydrogen from methane, including steam methane reforming coupled with CO_2 capture and storage (so called low-CO_2 or blue hydrogen) and methane pyrolysis (CO_2-free or turquoise hydrogen). The carbon footprint of these technologies is sensitive to the efficiency of carbon capture, CO_2 leakage, source of heat to run the process, fugitive methane emissions and natural gas supply chain due to the vicinity of deposits [2,3]. The conceptual difference of hydrogen production using steam methane reforming with carbon capture and storage from methane pyrolysis is a form of carbon by-product. The former technology generates CO_2. That requires permanent CO_2 storage, typically under supercritical conditions in geological formations. Leakage from storage sites is the major risk associated with CO_2 and it can be induced by geochemical reactions, pressure and temperature as well as poor cement cladding near a wellbore region [4]. The latter technology transforms methane into a solid carbon product, that is easier to handle, and store compared to CO_2, for instance, in concrete [5].

While the above-mentioned technologies can reduce carbon emissions, their benefits come at a cost of higher fossil resource consumption. The efficiency drop of steam methane reforming upon integration with carbon capture and storage is 5-14% [2], meaning more methane is required to compensate growing process needs. The consumption of methane is even larger when steam methane reforming is replaced by methane pyrolysis. During steam methane reforming, one molecule of methane can yield up to four molecules of hydrogen. The first step of the process is a reforming reaction, typically yielding a gas mixture containing hydrogen and CO. Water gas shift reaction is then applied as a second step to catalytically

convert CO in the presence of steam into CO_2 and generate more hydrogen. During methane pyrolysis, only two molecules of hydrogen are produced from one molecule of methane. That is, two times larger methane usage is required to reach the equivalent hydrogen outputs.

Reforming step: $CH_4 + H_2O = CO + 3H_2$ (1)

Water-gas shift step: $CO + H_2O = CO_2 + H_2$ (2)

Combined steam methane reforming: $CH_4 + 2H_2O = CO_2 + 4H_2$ (3)

Methane pyrolysis: $CH_4 = C + 2H_2$ (4)

How to mitigate intensified fossil resource consumption while decarbonizing hydrogen production? One way to achieve this goal is by partially replacing natural gas with alternative hydrocarbon sources. Biomass is one potential feedstock for hydrogen production. However, the concentration of hydrogen in producer and pyrolysis gases (i.e. from gasification and pyrolysis, respectively) is relatively low due to the high O/C molar ratios. This leads to exergy losses [6] and co-generation of large quantities of carbon oxides [7], reflecting on hydrogen separation cost and potential need for CO_2 capture and storage.

An alternative source of hydrogen is plastic waste. Global plastic consumption is growing. So does the amount of discarded plastic waste and associated pollution due to leakage of plastics into the environment [8]. Plastic waste is recognized as a promising feedstock for hydrogen production via gasification and pyrolysis-based technologies. Lopez at al. [9] reviewed thermochemical technologies for plastic waste utilization and pointed out several challenges related to gasification, including tar generation and dilution of hydrogen stream by other products. The authors highlighted advantages of pyrolysis-reforming process, yielding syngas with higher hydrogen concentrations and low tar contents. In recent years, pyrolysis-chemical vapor deposition process was widely studied [10]. Haggar et al. [11] demonstrated the production of gas over a catalyst with hydrogen content up to 81 vol.% using low-density polyethylene (LDPE) as a feedstock. The obtained carbon deposits were in a form of multi-walled carbon nanotubes. Due to relatively low temperatures of chemical vapor deposition stage (typically, below 800 °C), the complete conversion of hydrocarbons was not attainable, and the product gas contained methane and other by-products [10-12]. In another

study, thermal plasma pyrolysis was applied for the decomposition of plastics. Even though plasma arc temperatures could reach above 11,000 K, the obtained hydrogen-rich gas contained residues of undecomposed hydrocarbon compounds (51.2-79.4 vol.% H_2 and 20.6-47.4 vol.% C_1-C_5 hydrocarbon compounds, depending on the feedstock and conditions) [13]. According to hydrogen supply chain analysis data, purification stage can contribute up to 30% of operation costs with higher costs expected for the lower purity hydrogen streams [14]. Therefore, further improvements in the processing of plastics are required in order to obtain cost competitive hydrogen.

The objective of this study was to investigate the production of concentrated hydrogen streams (above 90 vol.% H_2) with nearly complete hydrocarbon decomposition (below 1 vol.% C_1-C_5 hydrocarbon compounds) using thermal pyrolysis (thermolysis) of non-condensable pyrolysis gas from plastics. In this sense, the process resembles CO_2-free or turquoise hydrogen production from natural gas, except natural gas is substituted by plastic waste in order to reduce consumption of fossil resources. While thermolysis has been extensively studied for the decomposition of single hydrocarbon gases, including pure methane [15, 16], ethane [17] and propane [18], as well as natural gas [189], pyrolysis oils from biomass [20] and tires [21], there are limited data about the application of this process towards conversion of pyrolysis gas from plastics using non-plasma process. Pure LDPE and mixtures of real-world post-consumer plastics containing polyethylene terephthalate (PET) were used. The effects of feedstock type and thermolysis temperature (1200-1500 °C) on the properties of hydrogen gas and solid carbon were investigated. Special attention was given to the characterization of carbon black in order to gain insights about potential valorization pathways of this material.

2. Materials and methods

2.1 Plastics

Pure LDPE (Lotte Chemical Titan, denoted as LDPE) and a mixture of sorted post-consumer plastic packaging, primarily composed of polyethylene and propylene (denoted as

mixed plastics, MP) were used in the study. Polyethylene terephthalate bottles (denoted as PET) were added to MP to investigate the influence of PET on hydrogen and solid carbon evolution. Although recycling rates of PET are generally high, it is not always profitable or practical to recycle PET items due to contamination or lack of infrastructure and other challenges [22]. In such circumstances, thermal treatment of mixed plastics containing PET could be an alternative option. LDPE was used in the form of pellets. MP and PET were shredded into flakes prior to experiments. The properties of three types of plastics are shown in Table 1. Due to the heterogeneity and small quantities of sample taken for the elemental analysis (several mg), the experimental errors for C and H contents of MP were higher compared to LDPE and PET. The higher ash content in MP could be due to the presence of inorganic fillers and metallized packaging in the plastic waste. MP was mixed with PET to prepare a mixture containing 60 wt.% MP + 40 wt.% PET (denoted as 60MP40PET).

Table 1. Characteristics of plastics.

Properties[a]	LDPE	MP	PET
C, wt.%	84.2±0.1	79.1±8.9	62.0±0.1
H, wt.%	15.4±0.3	14.1±2.0	4.0±0.2
N, wt.%	<0.1	0.2±0.2	<0.1
S, wt.%	0.4±0.4	0.4±0.2	<0.1
Fixed carbon, wt.%	<0.1	0.6±0.3	6.2±1.4
Volatile matter, wt.%	99.7±0.1	96.5±0.6	93.8±1.4
Ash (550 °C), wt.%	<0.1	2.4±0.8	<0.1
Higher heating value, MJ/kg	46.5±0.2	39.4±0.8	23.0±0.2

[a] where applicable, the values are reported as averages ± standard deviations; C, H, N, S contents were determined by Elementar Vario El Cube; fixed carbon, volatile matter and ash content were determined by gravimetry in a muffle furnace; higher heating value was measured by IKA C2000 equipped with a 260 mL calorimetric bomb.

2.2 Experimental setup

The process flow diagram is shown in Fig. 1A. The conversion of plastic waste into hydrogen was decoupled into two stages: plastic pyrolysis and gas thermolysis. Pyrolysis stage refers to the thermal degradation of plastic waste in the absence of oxidizing gases and resulting in the formation of condensable liquid product (oil) and non-condensable gas (pyrolysis gas). The produced oil from plastic waste can potentially replace crude oil as a feedstock in refineries, e.g., in a steam cracker [23]. Therefore, only pyrolysis gas containing mainly C_1-C_5 and small quantities of C_{6+} compounds [24] was used for the valorization via thermolysis. Thermolysis refers to the thermal decomposition of hydrocarbon compounds containing in pyrolysis gas into a solid carbon product and hydrogen. Both plastic pyrolysis and hydrocarbon gas thermolysis are considered scalable technologies [19, 25]. The replacement of methane with plastic waste-derived gas provides means for defossilization of hydrogen production, while capture, utilization or storage of solid carbon can decarbonize the process.

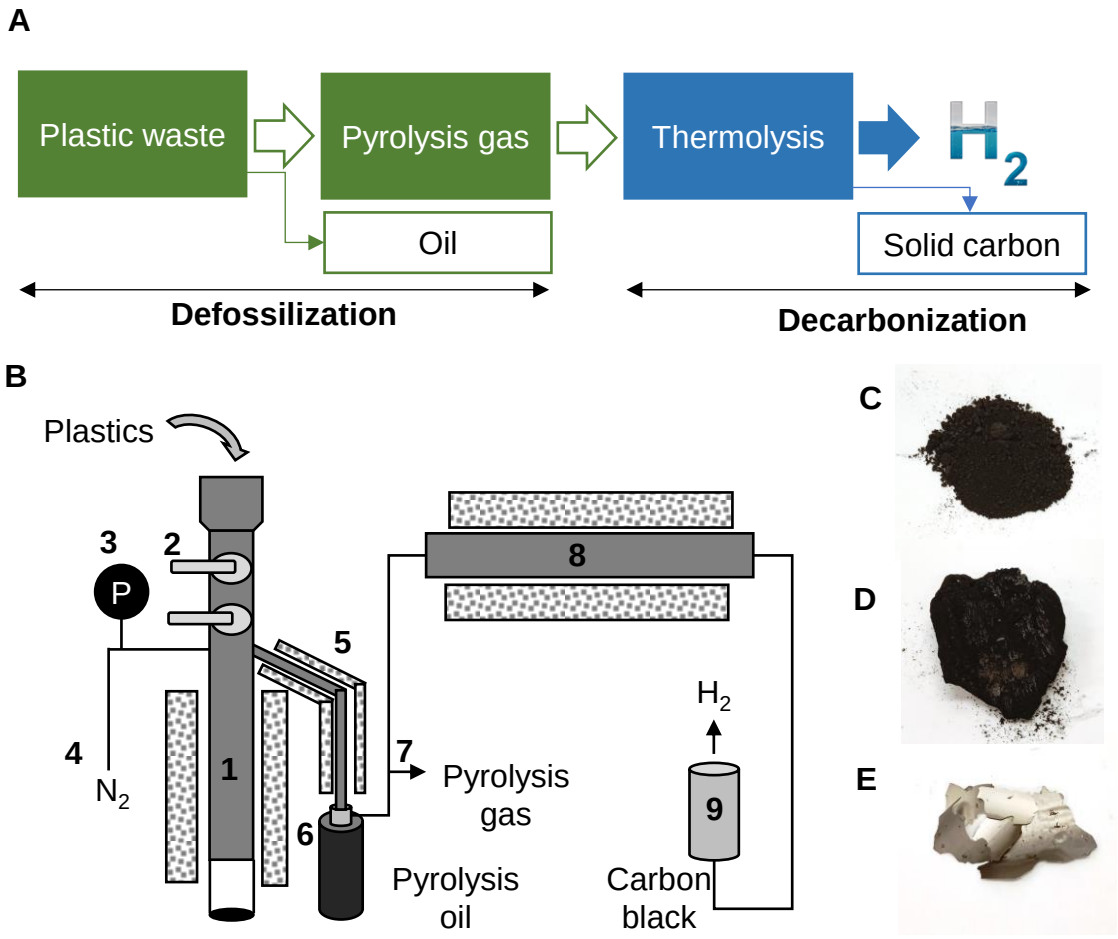

Fig. 1. (A) Process flow diagram of plastic waste-to-hydrogen comprising pyrolysis and thermolysis stages. (B) Experimental setup: 1 – plastic pyrolysis reactor, 2 – airlock valve, 3 – manometer, 4 – N_2 supply, 5 – cracking reactor, 6 – oil condenser, 7 – sampling port for pyrolysis gas, 8 – thermolysis reactor, 9 – filter. (C) Carbon collected from the particle filter, (D) carbon recovered from the thermolysis reactor and (E) carbon layer deposited on the inner wall of thermolysis reactor (MP, 1300 °C).

Fig. 1B shows the experimental setup. Plastic samples were fed into a stainless steel pyrolysis reactor pre-heated to 600 °C (15 g every 10 min). N_2 was supplied as a sweep gas and internal standard for the calculation of total gas volume using gas chromatography (50 mL/min). The produced volatile products were directed into a cracking reactor, comprising a hollow tube pre-heated to 600 °C. The purpose of cracking reactor was to increase the residence time of volatile pyrolysis products at high temperature to facilitate decomposition

into pyrolysis gas [26]. Liquid pyrolysis products were collected in a condenser maintained at ambient temperature (approx. 23 °C). The pyrolysis gas was directed via a pipeline into an alumina reactor pre-heated to 1200-1500 °C followed by a filter, separating solid carbon from product gas containing hydrogen (referred to as a product gas). The thermolysis reactor had an inner diameter of 5 cm and the reaction zone of 70 cm.

In a typical experiment, the pyrolysis and thermolysis reactors were pre-heated and purged with N_2 to remove air. Plastic pyrolysis was conducted semi-continuously by feeding 15 g of material every 10 min. Together with plastics, 50 mL/min of N_2 were continuously co-fed into the pyrolysis reactor. During 1 h of flow stabilization, pyrolysis gas by-passed the thermolysis reactor. After 1 h, the feeding of plastics and N_2 into the pyrolyzer continued at the same rates. A sample of pyrolysis gas was collected into a gas bag and the stream of pyrolysis gas was switched from the by-pass to the thermolysis reactor. The collection of carbon at the outlet of the thermolysis reactor was started immediately after switching to the thermolysis reactor and continued for 30 min. The collection of product gas was started 5 min later to allow for the displacement of N_2 in the thermolysis reactor with produced H_2. The collection of product gas continued for 25 min. Then, the stream of pyrolysis gas was switched back to the by-pass and one more sample of pyrolysis gas was collected in a gas bag. The filter was cleaned to remove solid carbon and the thermolysis process was conducted 2 more times before cooling the pyrolysis and thermolysis reactors. In addition to carbon collected from the filter, carbon samples recovered from the thermolysis reactor were also analyzed. Fig. 1C, 1D and 1E show the three specimens of solid carbon samples: a powder from the particulate filter, a bulk agglomerate from the thermolysis reactor (resembling a plug sample from thermal methane cracking reported in [27]) and a thin film grown on the inner surface of the thermolysis reactor. The first two carbon samples have black color, while the film is shiny and silvery. For each set of conditions, the experiment was conducted twice, resulting in the collection of 6 samples of product gas and 8 samples of pyrolysis gas in total. Additionally, pyrolysis experiments were conducted three times for each feedstock to quantify the production of oil and solid residue. All results are reported as averages and the experimental errors are

expressed as standard deviations. Where applicable, the statistical significance of averages was evaluated using a two-tailed *t*-test with a confidence level of 95%.

2.3 Characterization of samples

Product and pyrolysis gases were characterized by a gas chromatograph with one flame ionization and two thermal conductivity detectors (customized 7890B, Agilent). The chromatograph was calibrated with a mixture containing 21 C_1-C_5 hydrocarbon compounds, CO, CO_2, H_2 and N_2. The flow rate of each component in a mixture was calculated by knowing the flow rate of N_2 and volumetric concentrations of the component and N_2. Hydrogen, carbon and oxygen contents (g/min) were determined from the volumes of components in pyrolysis and product gases. The production rates of product gas, solid carbon and hydrogen were calculated as:

Product gas (g/min) = m(H product gas) + m(C product gas) + m(O product gas) (5)

Solid carbon (g/min) = [m(C pyrolysis gas) – m(C product gas)]/[C determined by CHNS analysis] (6)

Hydrogen (g/min) = m(H product gas) (7)

The yields of product gas, solid carbon and hydrogen per mass of plastics were calculated by dividing production rate by feeding rate (i.e. 1.5 g/min plastics).

The yields of oil and solid residues from the pyrolysis reactor were calculated based on the masses of products divided by the mass of plastics used for experiments. The material balance was determined as the sum of yields of product gas, solid carbon, oil and solid residue.

Solid carbon samples were characterized by transmission electron microscopy (TEM, JEOL JEM-1400Plus) and field emission scanning electron microscopy (FESEM, JEOL JSM-7600F). The size distribution of solid carbon particles collected on the filter was determined by calculating diameters of 300-350 spherical particles from TEM images. A graphitization degree was analyzed by Raman spectroscopy (XploRA PLUS, Horiba Scientific) with a 532 nm laser excitation. C, H, N and S contents of solid carbon and oil were determined by

Elementar Vario El Cube. N_2 adsorption/desorption isotherms were measured by Quantachrome Autosorb-1 Analyzer at −196 °C. The Brunauer–Emmett–Teller (BET) model was used to determine the specific surface area of solid carbon. The total pore volume was calculated from N_2 uptake at P/P_0 = 0.95-0.96.

3. Results and discussion

3.1 Effect of plastic feedstock on product output

Pure LDPE was used as a reference material in this study. The distribution of products after the thermolysis at 1300 °C is shown in Table 2. The main output was oil (52 wt.%) followed by solid carbon (40 wt.%), product gas (9 wt.%) and negligible quantity of solid residue remaining in the pyrolysis reactor (<0.1 wt.%). Commercial pyrolysis processes optimized for oil production can yield 75-95 wt.% oil [25]. In this study, oil production was lower due to higher pyrolysis temperature and increased residence time. Hydrogen production from LDPE was 7 wt.%. This plastic showed better mass balance closure (101%) as compared to other two samples (80-99 %, depending on the experimental run). The decrease in mass recovery suggests that in case of real waste samples there could be other unaccounted compounds formed during the process. For example, volatile organic compounds or aerosols condensing along the lines.

Table 2. Product outputs from the plastic waste-to-hydrogen process.

Feedstock	LDPE	60MP40PET	MP			
Temperature (°C)	1300	1300	1200	1300	1400	1500
Product gas (wt.%)	9±1	21±3	10±2	9±2	13±2	10±1
Solid carbon (wt.%)	40±5	42±3	37±2	41±8	53±2	36±6
Oil (wt.%)	52±7	8±1		24±7		

Solid residue (wt.%)	<0.1	12±6		10±6		
Mass balance (wt.%)	101	84	81	84	99	80
Hydrogen (wt.%)	7±1	5±2	6±1	6±1	9±1	7±1

Compared to LDPE, pyrolysis of MP and 60MP40PET at 600 °C resulted in the formation of more solid residue in pyrolysis reactor and less oil. Since the quantities of solid residue (i.e. 10 and 12 wt.% from MP and 60MP40PET) were higher than the ash contents of the individual polymers (i.e. 2.4 and 0.1 wt.% for MP and PET), the specimens contained both ashes and coke formed by carbonization of organic material under the pyrolysis conditions. The lower oil yields from MP and 60MP40PET (i.e. 24 and 8 wt.%) were probably caused by the differences in plastic feedstock composition. Based on the CHNS analysis, oil samples mainly consisted of carbon and hydrogen atoms (Table S1). The contents of these elements were comparable regardless of plastic feedstock. In case of the PET addition, the decrease in oil yield is well documented [28, 29]. One reason is the increased formation of CO and CO_2 from PET, which was also observed by the gas chromatography of pyrolysis gas from 60MP40PET (Fig. 2A). Another reason is the production of sublimated organic solids, such as benzoic and terephthalic acids, that may condense on cold reactor walls or form aerosols, which by-pass the oil trap and accumulate in downstream gas lines.

The composition of pyrolysis gas flowing into the thermolysis reactor is shown in Fig. 2A and Fig. 2B. Notably, the H_2 concentration was only 7-12 vol.%, while the total content of hydrocarbon compounds was 41-84 vol.%, depending on the plastic feedstock. After the thermolysis at 1300 °C, hydrocarbon compounds were decomposed generating 40-42 wt.% of solid carbon (Table 2). Based on the similar quantities of solid carbon, there was little if any influence of the feedstock composition on carbon formation in this study. However, the effect of plastics on the generation of product gas was significant. The quantities of product gas after

thermolysis of MP and LDPE were 9 wt.% per mass of plastic feed, which is much lower compared to 60MP40PET (i.e. 21 wt.% per mass of plastic feed). The overall recovery of molecular hydrogen from the three samples was not statistically different (i.e. the yield of hydrogen was 7±1, 6±1 and 5±2 wt.% for LDPE, MP and 60MP40PET according to Table 2). The remaining species in product gas accounted for 2, 3 and 16 wt.% for LDPE, MP and 60MP40PET and included traces of C_1-C_5 hydrocarbon compounds, N_2 and CO (Fig. 2C and Fig. 2D). Although the volumetric percentages of the above mentioned impurities are lower compared to hydrogen, these compounds are heavier. Therefore, even small volumetric concentrations of impurities can make a large impact on the yield of product gas expressed on a mass basis. The contribution becomes more prominent with the increase in concentration of gas impurities as it can be observed in case of the product gas from 60MP40PET, containing 19.3 vol.% CO (Fig. 2C).

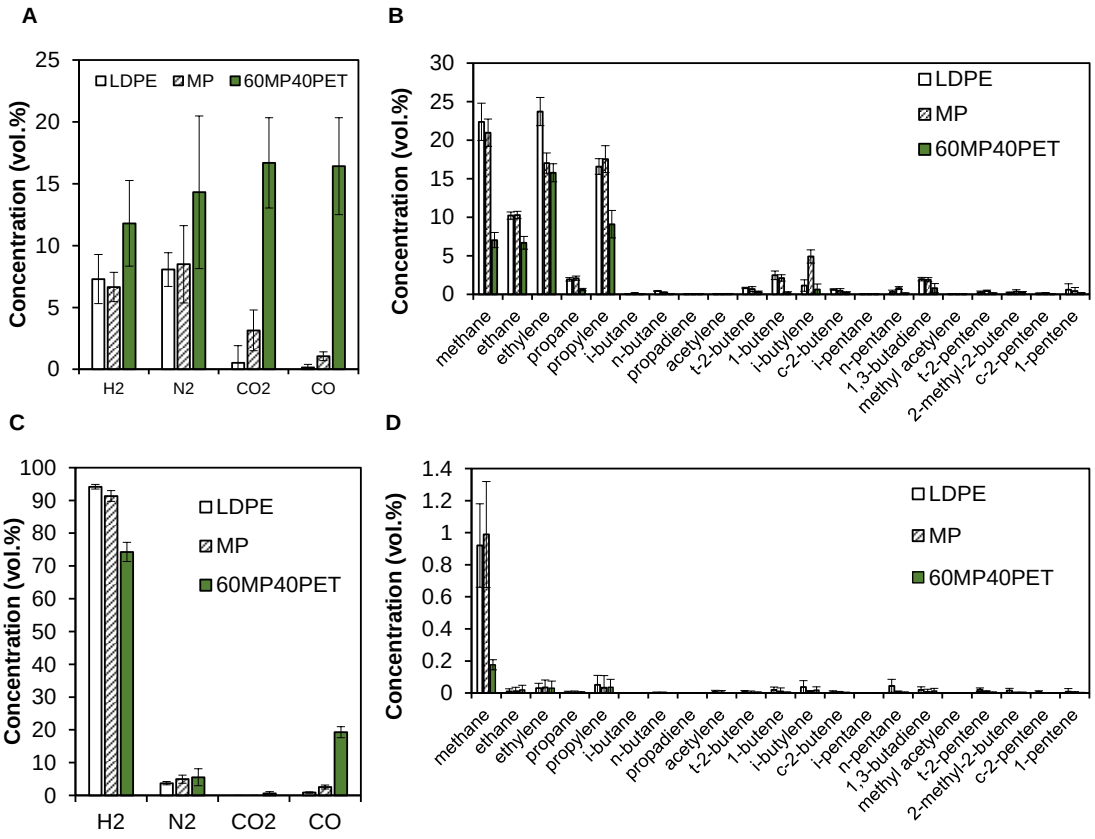

Fig. 2. Pyrolysis (A, B) and product gases (1300 °C) (C, D) from the four types of plastics: (A, C) H_2, N_2, CO_2 and CO and (B, D) C_1-C_5 hydrocarbon compounds.

According to Fig. 2C, the volumetric hydrogen concentration in the product gas was the highest in case of LDPE (94.2 ± 0.7 vol.%) followed by MP (91.3 ± 1.7 vol.%) and 60MP40PET (74.3 ± 2.9 vol.%). Although CO_2 was present in the pyrolysis gas of MP and 60MP40PET samples (Fig. 2A), after thermolysis at 1300 °C, it was converted into CO, indicating the oxidation of hydrocarbon compounds and/or solid carbon by CO_2 in the thermolysis reactor. CO_2 could also react with H_2 via a reverse water gas shift reaction producing CO and H_2O. The residues of N_2 gas used as an internal standard for volume calculation can be seen in all gas samples and accounted for no more than 5.5 vol.% (Fig. 2C). The elimination of N_2 usage as an external standard for volume calculation can improve hydrogen purity further. For all samples, almost complete decomposition of C_1-C_5 hydrocarbon compounds was achieved at 1300 °C (Fig. 2D) with the most stable hydrocarbon species being methane as suggested by the highest volumetric concentration. Compared to hydrocarbon compounds with larger number of carbon atoms, methane has the stronger C-H bond, making it more difficult to decompose into C and H_2 [30]. Fig. 3 shows the production rates of pyrolysis and thermolysis gases (1300 °C) from the three types of plastics. The output of pyrolysis gas was 600-800 mL/min, depending on plastic feedstock. Upon the thermolysis stage, the decomposition of hydrocarbon compounds into solid carbon and hydrogen occurred. According to Fig. 2B, the hydrocarbon compounds in the pyrolysis gas were mainly alkanes and alkenes with general formulas C_nH_{2n+2} and C_nH_{2n}, where n is the number of carbon atoms. During the thermal decomposition of alkanes and alkenes, (n+1) and n molecules H_2 per n number of carbon atoms are formed, respectively. Furthermore, each CO_2 molecule produces 2 molecules of CO during the reaction with hydrocarbon compounds and solid carbon. Due to these reactions, the volume of product gas after thermolysis increased to 1000-1350 mL/min, depending on the feedstock.

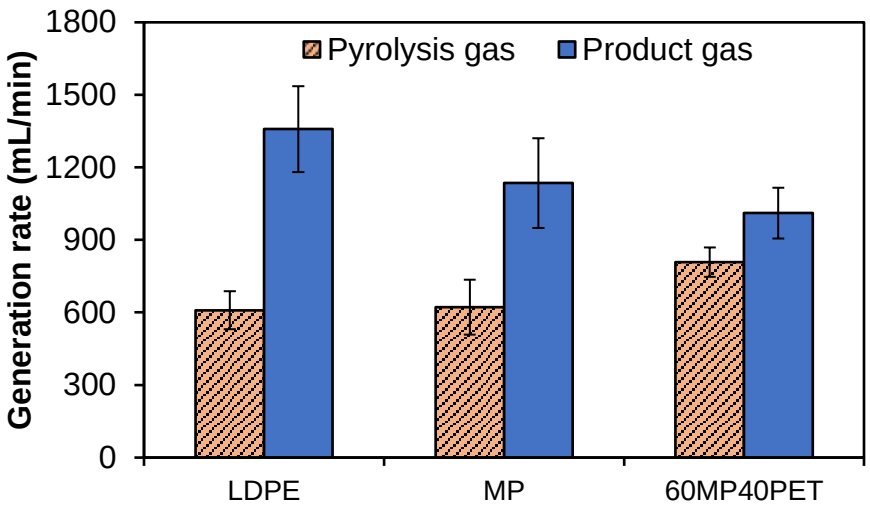

Fig. 3. Influence of plastic feedstock on the generation of pyrolysis and product (1300 °C) gases.

Apart from the two-stage pyrolysis-thermolysis process described in this study, two commonly investigated thermal technologies were pyrolysis-steam reforming and pyrolysis-chemical vapor deposition (CVD) as reviewed in [10] and compared in Table 3. The H_2 purity from polypropylene pyrolysis-steam reforming could reach up to 66 vol.% only [31], due to dilution by released CO and CO_2. The reported H_2 purity obtained by pyrolysis-chemical vapor deposition of LDPE at 700 °C was up to 81 vol.%, which is lower than that shown in Fig. 2C for LDPE and MP [11]. The lower hydrogen concentration (~80 vol.%) was also achieved by microwave-initiated pyrolysis-chemical vapor deposition of high-density polyethylene [32]. Thermal plasma pyrolysis of polyethylene, polypropylene, polyvinyl chloride and acrylonitrile butadiene styrene was reported to produce lower product gas purities with gas containing 51.2-79.4 vol.% H_2 [13]. Pyrolysis-thermolysis is more energy intensive process than those described in [10-13, 31-33] as it is conducted at higher temperatures. H_2 yield is lower than from pyrolysis-steam reforming as the only source of H_2 molecules is plastic feedstock but higher than from pyrolysis-CVD due to higher hydrocarbon conversion efficiency. The data above suggest that one of the main advantages of pyrolysis-thermolysis process is that it can produce the gas with higher H_2 purity (subject to the plastic feedstock composition and,

especially, PET content, yielding CO). Furthermore, metal catalysts that are prone to deactivation are not required for the thermolysis stage, thus allowing for the lower raw material footprint. It also avoids contamination of solid carbon by catalyst residues and eliminates carbon purification stage compared to pyrolysis-CVD process. These trade-offs should be considered when analysing pros and cons of technologies for hydrogen generation and solid carbon capture from plastics.

Table 3. Thermal two-stage technologies for hydrogen recovery from plastic waste [10].

	Pyrolysis-steam reforming	Pyrolysis-CVD	Pyrolysis-thermolysis
H_2 purity	Up to 66 vol.% [31]	Up to 81 vol.% [13]	Up to 94.2 vol.% [This study]
H_2 yield	Up to 38 g/100 g plastics [32]	Not reported	Up to 6-9 g/100 g plastics [This study]
Typical temperature range	600-900 °C	500-900 °C	1200-1500 °C
Catalyst	Required for the reforming stage	Required for the CVD stage (short catalyst life-time)	Not required
Main by-products	CO, CO_2	Carbon nanotubes, carbon nanofibers, CH_4	Carbon black

3.2 Influence of thermolysis temperature on product gas

MP sample was used to investigate the effect of thermolysis temperature in the range of 1200-1500 °C on the gas composition. In all gas samples, hydrogen was the main component with the lowest concentration at 1200 °C (89.8 ± 0.4 vol.%), reaching the maximum

at 1400 °C (94.0 ± 0.5 vol.%) (Fig. 4A). The contents of N_2 and CO were 3.0-4.9 and 1.8-3.0 vol.%, respectively at 1200-1500 °C. Among hydrocarbon compounds, methane was the predominant species due to the high stability of the molecule (Fig. 4B). The largest methane content was observed in the product gas obtained at 1200 °C (4.1 ± 0.5 vol.%) followed by 1300 °C (1.0 ± 0.3 vol.%), 1400 °C (0.1 ± 0.1 vol.%) and 1500 °C (0.1 ± 0.1 vol.%). The concentration of C_2-C_5 hydrocarbon compounds at 1200 °C was 0.3 vol.% and did not exceed 0.1 vol.% at higher temperatures. According to these results, at the studied temperatures, the decomposition of methane was the limiting step determining the overall conversion efficiency of hydrocarbon compounds in plastic pyrolysis gas into hydrogen. For the experimental setup and conditions used in this study, almost complete hydrocarbon conversion containing in the pyrolysis gas was achieved at around 1400 °C. The obtained temperature was close to the temperature of complete methane splitting using a non-catalytic 10 kW solar powered thermolysis reactor (1450 °C) [34]. The kinetic data for methane decomposition at 1427 °C showed that residence time above 0.03 s^{-1} assures nearly complete methane conversion [35]. Based on the dimensions of reactor and product gas volume provided in Fig. S1 (assuming no deviation from ideal gas behavior), it can be calculated that the residence time at 1300-1500 °C was 9-14 s, exceeding the reported values. Thus, it can be concluded that the thermolysis time was sufficient to decompose most of methane containing in the pyrolysis gas.

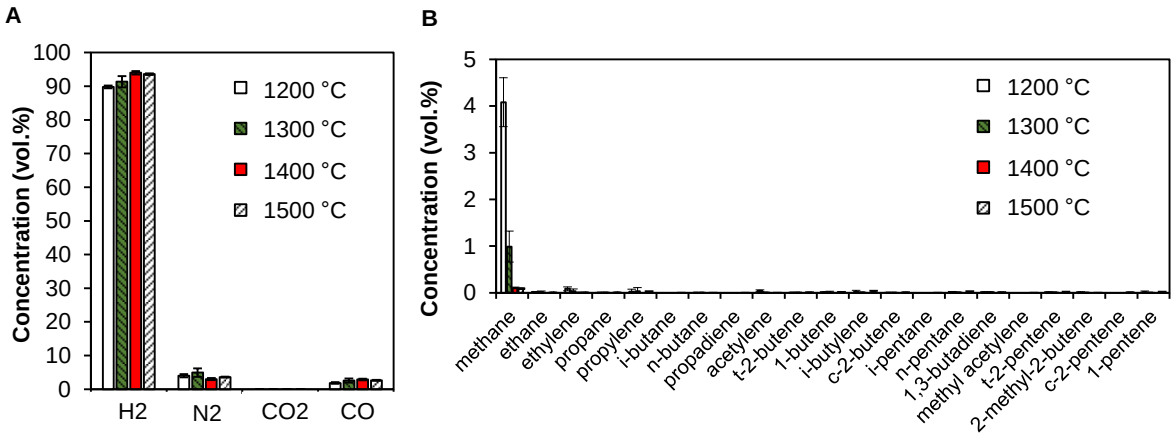

Fig. 4. Influence of thermolysis temperature on product gas composition (MP feedstock): (A) H_2, N_2, CO_2 and CO and (B) C_1-C_5 hydrocarbon compounds.

3.3 Properties of solid carbon from the thermolysis process

Solid carbon was the main by-product from hydrogen generation and is the most abundant output from the thermolysis of plastic pyrolysis gas regardless of the plastic type and process temperature (Table 2). Characterization of solid carbon is important for determining potential applications of this material to improve economic viability of the plastic waste-to-hydrogen process. Fig. 5 shows the morphologies of the three solid carbon types produced by thermolysis of MP feedstock at 1300 °C. Based on the FESEM and TEM images, there were distinct differences in the material structure, attributed to the various growth mechanisms. Furthermore, the morphologies were different from those synthesized via catalytic chemical vapor deposition of pyrolysis gas from plastics at lower temperatures, typically yielding filamentous carbon, such as multi-walled carbon nanotubes [10-12, 36], few-walled carbon nanotubes [37, 38] and nanofibers [36]. Solid carbon collected from the particle filter consisted of spheroidal aggregates, resembling typical morphology of carbon black [39, 40]. Taken into consideration the residence time of product gas in the thermolysis reactor (i.e. 9-14 s), the formation of carbon black aggregates was accomplished within several seconds. The growth of carbon black is associated with the formation in a gas phase of reactor [41] and involves three stages [39]:

(1) Nucleation of carbon black precursors and carbon black inception, including the transformation of gas molecules into carbon particles with dimensions in order 1-2 nm.

(2) Aggregation of nucleated particles due to collision, resulting in the formation of larger spheroidal particles with sizes in the nanometer range.

(3) Aggregation or agglomeration of spheroidal particles into chains.

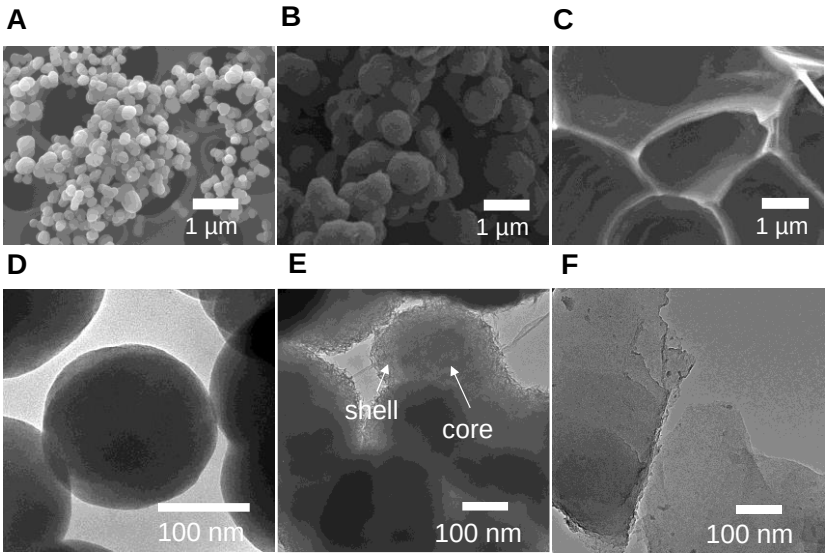

Fig. 5. FESEM (top) and TEM (bottom) images of solid carbon particles after thermolysis (MP, 1300 °C): (A, D) Carbon collected from the particle filter, (B, E) carbon recovered from the thermolysis reactor and (C, F) carbon layer deposited on the inner wall of thermolysis reactor.

On the contrary, solid carbon recovered from the thermolysis reactor was predominantly composed of fused spheroidal particles coated with a layer of attached pyrolytic carbon (Fig. 5B, 5E). The differences in the density of two carbon types can be observed in the TEM image with a spheroidal core, having higher density and darker color, and an outer shell, having lower density and lighter color. (Fig. 5E). The imaging of different areas of sample (Fig. S2) shows that the thickness and density of the outer layers formed on the core surfaces vary, suggesting that the core is likely formed first, while the shell is deposited thereafter. The appearance of core structures is similar to the spheroidal carbon black aggregates collected from the filter. The surface of carbon can act as a site for solid-gas interactions, promoting the decomposition of hydrocarbon compounds at temperatures as low as 750 °C 42]. These reactions could result in the formation of shell composed of pyrolytic carbon on the surface of carbon black particles. A previous study of carbon formation during methane pyrolysis also suggested that the growth rate of pyrolytic carbon on surfaces is slower compared to the growth of carbon black aggregates [41]. Therefore, the growth mechanism of carbon collected

from the thermolysis reactor could be described as having one more step in addition to those for carbon black aggregates:

(4) Pyrolytic carbon deposition on the surface of carbon black particles.

The morphology of shiny silvery film grown on the surface of reactor walls is shown in Fig. 5C and 5F. Unlike the other two types of carbon, this material contained only aspherical structures. The surface of carbon was uneven and composed of stacked pyrolytic coke layers. The layers had distinct sharp edges. The stacking of several layers can be observed from the color gradient in the TEM image with the lighter areas corresponding to the thinner carbon layer and the darker area to the thicker carbon deposits (Fig. 5F). Similar to the carbon shell formed in the previous carbon sample, the growth of this carbon type was associated with the surface reactions. The differences in morphologies were caused by the different structure of underlying surfaces (i.e. the surface of carbon black against alumina) as the composition and properties of surface are crucial factors for carbon growth [41-43].

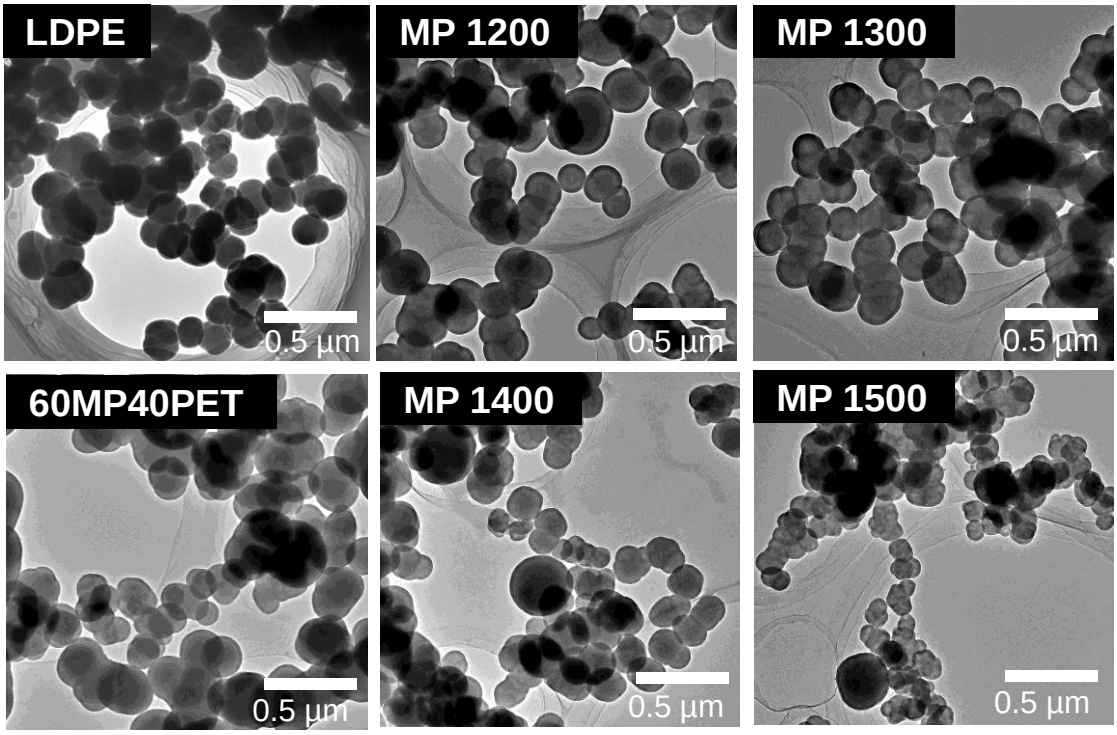

Fig. 6. TEM images of carbon black aggregates: LDPE and 60MP40PET samples were obtained by the thermolysis at 1300 °C and MP by the thermolysis at 1200, 1300, 1400 and 1500 °C.

As it was shown above, carbon black particles trapped in the thermolysis reactor played the important role in hydrocarbon decomposition (Fig. 5E and Fig. S2). Apart from that, carbon black is a marketable product that is widely used as a manufacturing additive [39]. The production of carbon black is around 15 million tonnes per year globally with 73% carbon black being used in automobile tires, 20% in non-tire rubber products and 7% in paints, coatings, inks, plastics and other products [44]. Therefore, the properties of carbon black aggregates collected from the filter were comprehensively investigated. Fig. 6 shows TEM images of carbon black aggregates from the three types of plastics. The aggregates were composed of predominantly spheroidal and ellipsoidal carbon particles. Some of the particles were fused together in randomly arranged clusters. The clusters were aligned in linear and branched morphologies. Such carbon black aggregates were obtained from all studied plastics and at all studied thermolysis temperatures.

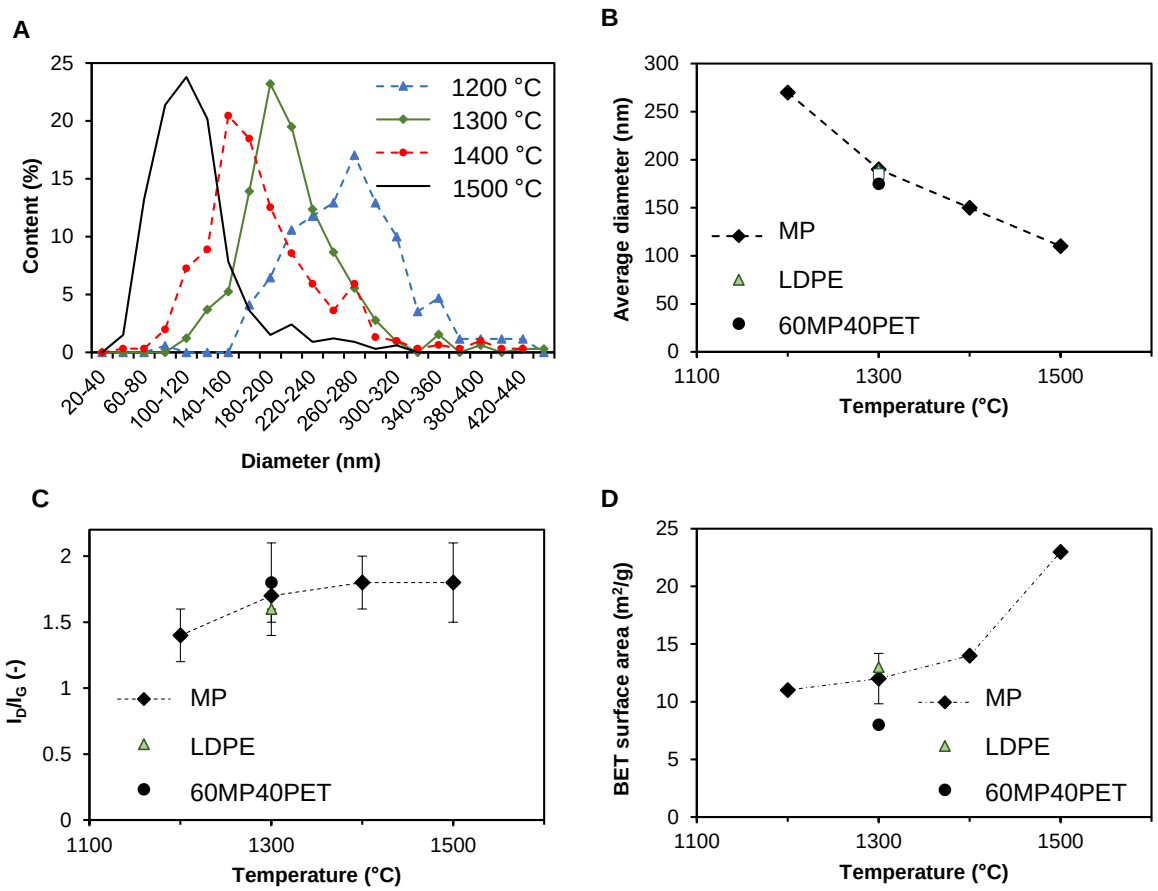

Fig. 7. (A) Effect of thermolysis temperature on diameter distributions of spherical carbon black aggregates from MP. Effect of thermolysis temperature and plastic feedstock on (B) average diameters of spherical carbon black aggregates, (C) I_D/I_G values and (D) BET surface areas (The lines are only to guide the eye. Where applicable, the error bars represent standard deviations based on at least 3 measurements).

To gain a better insight about the sizes of carbon black aggregates, the diameters of 300-330 spheroidal particles from each sample were measured using TEM images. The influence of thermolysis temperature on the diameters of particles from MP is shown in Fig. 7A. The lowest temperature (1200 °C) resulted in the particles with the largest diameters in the range of 160-360 nm. With the increase in temperature, the size distributions shifted to smaller particle ranges (i.e. 20-200 nm at 1500 °C). For all samples, the width (i.e. the distance between smallest and largest particles) of size distribution remained comparable to approx. 180-200 nm. The gradual decrease in average diameters of spherical aggregates from 270

nm to 110 nm with the increase in thermolysis temperature is demonstrated in Fig. 7B for the MP sample. The similar influence of temperature was reported previously for the growth of carbon black from ethylene [45] and benzene [46], suggesting that the growth mechanism of carbon black from pyrolysis gas of plastics is consistent with other studied precursors. The same figure shows the average diameters of the two other types of plastics at 1300 °C. Unlike temperature, the feedstock composition had little if any effect on the size of carbon black particles since the average diameters of carbon black from MP, LDPE and 60MP40PET were comparable. At the studied concentration in pyrolysis gas, the CO_2 released during PET decomposition had no significant impact on the size of carbon black aggregates.

The influence of thermolysis temperature and plastic feedstock on the properties of carbon black aggregates was further investigated using elemental analysis, Raman spectroscopy and N_2 adsorption. The compiled results are provided in Table S2. The content of carbon in the samples was 98.8-99.0 wt.% with the remaining mass attributed to H, N and S, indicating the high purity of carbon material. The low H/C ratio of 0.005-0.009 for the produced sample is one of the characteristics that distinguish carbon black from soot, having H/C ratio of approx. 1 [47]. Raman spectra of the samples had typical D- and G-bands at 1350 and 1560 cm^{-1}, corresponding to defective and graphitic regions in carbon crystals (Fig. S3). In the Raman spectrum of pyrolytic graphite, only G-band can be found as the A_{1g} vibrational mode giving rise to the D-band is inactive in graphite crystals [48]. The intensity of D-band increases with the disorder of material structure. The degree of graphitization/disorder can be characterized by the ratio of areas of D- and G-bands I_D/I_G. The lower is the I_D/I_G ratio, the higher is the graphitization degree. According to Fig. 7C, the I_D/I_G ratios for carbon black aggregates were 1.4-1.8, indicating discontinuity and defectiveness of carbon crystals. These values are similar to the reported ones for some thermal and furnace carbon blacks produced at industrial scale (i.e. 1.3-1.6) [49]. The differences between I_D/I_G ratios of carbon black aggregates from plastic pyrolysis gas were within the experimental error range, suggesting the consistent graphitization degree regardless of the selected thermolysis temperatures and plastic feedstock. N_2 adsorption-desorption isotherms of carbon black aggregates from plastic

pyrolysis gas are shown in Fig. S4. All isotherms were Type II without hysteresis loops, indicating that the N_2 physisorption predominantly followed a monolayer-multilayer adsorption unrestricted by pores and typical for non-porous materials, including non-porous carbon blacks [50]. BET specific surface areas of carbon black aggregates from the three types of plastics obtained at 1300 °C were between 8 and 13 m^2/g (standard deviation ±2 m^2/g) (Fig. 7D). The thermolysis of pyrolysis gas from MP at 1200-1400 °C resulted in the comparable values of BET surface areas between 11 and 14 m^2/g. The main change in the N_2 adsorption was observed when the temperature of thermolysis was increased to 1500 °C as suggested by the BET surface area of 23 m^2/g of the carbon black sample from MP. The obtained surface areas are consistent with those for groups 7-9 of commercial carbon blacks classified for usage in rubber [51]. Such carbon blacks are considered medium to low grade reinforcement fillers in rubber production (subject to performance testing) [52]. Based on the characterization of size, elemental composition, graphitic structure and surface area, carbon black aggregates obtained from plastic pyrolysis gas could potentially serve as sustainable substitutes of commercial carbon blacks obtained from fossil hydrocarbon sources. Alternatively, the recovered carbon can be used for the development of new applications, such as a filler and carbon storage material in concrete [5], carbon-based environmentally friendly sensors [53], and electrochemical CO_2 reduction electrodes [54].

4. Conclusions

The recovery of 5-9 wt.% molecular H_2 per mass of plastic feedstock was demonstrated using three types of plastics in an integrated process comprising pyrolysis (600 °C) and thermolysis reactors (1200-1500 °C). Other products included solid residue and oil from the pyrolysis reactor, as well as solid carbon and product gas impurities produced in the thermolysis reactor. LDPE and MP could produce H_2 with exceptionally high gas purity of 89.8-94.0 vol.%, which could be further improved by eliminating the usage of N_2 (3-5 vol.% residual content, used as an internal standard and sweeping gas). The purity of H_2 was detrimentally influenced by the presence of PET in plastics due to the dilution by CO, indicating that PET

sorting could be advantageous prior to the plastic waste-to-hydrogen conversion. Based on thermolysis experiments at 1200-1500 °C, the decomposition of methane containing in the pyrolysis gas from plastics was the limiting reaction step during H_2 production. Three types of solid carbon were produced in the thermolysis reactor, namely carbon black collected at the outlet of reactor by a particle filter, fused carbon black aggregates coated with a layer of pyrolytic carbon and a carbon film coated on the inner reactor wall. Among these types of carbon, the carbon black aggregates collected on the particle filter have the valorization potential, while the applications for the other two types of carbon have to be yet identified. The carbon black samples from plastics were comparable to grade 7-9 commercial carbon blacks used as low and medium reinforcement fillers in rubber production. Variations in plastic feedstock had little if any effect on carbon black properties, while high thermolysis temperature (1500 °C) was beneficial for the reduction of particle sizes and increase in the surface area of aggregates.

Acknowledgements

The researchers would like to thank Singapore Energy Centre (SgEC) and DII Collaborative Graduate Program for financial support. This research / project is supported by the National Research Foundation, Singapore, and PUB, Singapore's National Water Agency under its RIE2025 Urban Solutions and Sustainability (USS) (Water) Centre of Excellence (CoE) Programme, awarded to Nanyang Environment & Water Research Institute (NEWRI), Nanyang Technological University, Singapore (NTU).

Disclaimer

Any opinions, findings and conclusions or recommendations expressed in this material are those of the author(s) and do not reflect the views of National Research Foundation, Singapore and PUB, Singapore's National Water Agency.

References

[1] Weger L, Abanades A, Butler T, Methane cracking as a bridge technology to the hydrogen economy, Int J Hydrog Energy 2017;42:720-731.

[2] Hermesmann M, Müller TE, Green, turquoise, blue, or grey? Environmentally friendly hydrogen production in transforming energy systems, Prog Energy Combust Sci 2022;90:100996.

[3] Parkinson B, Tabatabaei M, Upham DC, Ballinger B, Greig C, Smart S, McFarland E, Hydrogen production using methane: Techno-economics of decarbonizing fuels and chemicals, Int J Hydrog Energy 2018;43:2540-2555.

[4] Gholami R, Raza A, Iglauer S, Leakage risk assessment of a CO_2 storage site: A review, Earth-Sci Rev 2021;223:103849.

[5] Li J, Spanu L, Heo J, Zhang W, Gardner DW, Carraro C, Maboudian R, Monteiro PJM, Sequestration of solid carbon in concrete: A large-scale enabler of lower-carbon intensity hydrogen from natural gas, MRS Bulletin 2021;46:680-686.

[6] Prins MJ, Ptasinski KJ, Janssen FJJG, From coal to biomass gasification: Comparison of thermodynamic efficiency, Energy 2007;32:1248-1259.

[7] Arregi A, Amutio M, Lopez G, Bilbao J, Olazar M, Evaluation of thermochemical routes for hydrogen production from biomass: A review, Energ Convers Manage 2018;165:696-719.

[8] Geyer R, Jambeck JR, Law KL, Production, use, and fate of all plastics ever made, Sci Adv 2017;3:e1700782.

[9] Lopez G, Artetxe M, Amutio M, Alvarez J, Bilbao J, Olazar M, Recent advances in the gasification of waste plastics. A critical overview, Renew Sust Energ Rev 2018;82:576-596.

[10] Williams PT, Hydrogen and carbon nanotubes from pyrolysis-catalysis of waste plastics: A review, Waste Biomass Valor 2021;12:1-28.

[11] Haggar AM, Awadallah AE, Aboul-Enein AA, Sayed GH, Correlation between the as-grown carbon nano tubes and prolonged activity toward hydrogen production over Co–Mo/MgO, Mater Chem Phys 2022;288:126386.

[12] Veksha A, Mohamed Amrad MZB, Chen WQ, Binte Mohamed DK, Tiwari SB, Lim TT, Lisak G, Tailoring Fe_2O_3–Al_2O_3 catalyst structure and activity via hydrothermal synthesis for carbon nanotubes and hydrogen production from polyolefin plastics, Chemosphere 2022;297:134148.

[13] Mohsenian S, Esmaili MS, Fathi J, Shokri B, Hydrogen and carbon black nano-spheres production via thermal plasma pyrolysis of polymers, Int J Hydrog Energ 2016;41:16656-16663.

[14] Wickham D, Hawkes A, Jalil-Vega F, Hydrogen supply chain optimisation for the transport sector – Focus on hydrogen purity and purification requirements, Appl Energy 2022;305:117740.

[15] Msheik M, Rodat S, Abanades S, Experimental comparison of solar methane pyrolysis in gas-phase and molten-tin bubbling tubular reactors, Energy 2022;260:124943.

[16] Boretti A, Concentrated solar energy-driven carbon black catalytic thermal decomposition of methane. Int J Energy Res 2021;45:21497-21508.

[17] Cassady SJ, Choudhary R, Pinkowski NH, Shao J, Davidson DF, Hanson RK, The thermal decomposition of ethane, Fuel 2020;268:117409.

[18] Kang J, Ran J, Niu J, Shi J, He J, Yang Z, Experimental and theoretical study on propane pyrolysis to produce gas and soot, Int J Hydrog Energ 2019;44:22904-22918.

[19] Schneider S, Bajohr S, Graf F, Kolb T, State of the art of hydrogen production via pyrolysis of natural gas, ChemBioEng Reviews 2020;7:150-158.

[20] Toth P, Vikström T, Molinder R, Wiinikka H, Structure of carbon black continuously produced from biomass pyrolysis oil, Green Chem 2018;20:3981.

[21] Okoye CO, Jones I, Zhu M, Zhang Z, Zhang D, Manufacturing of carbon black from spent tyre pyrolysis oil – A literature review, J Clean Prod 2021;279:123336.

[22] Smith RL, Takkellapati S, Riegerix RC, Recycling of plastics in the United States: Plastic material flows and polyethylene terephthalate (PET) recycling processes, ACS Sustainable Chem. Eng. 2022;10:2084-2096.

[23] Kusenberg M, Faussone GC, Thi HD, Roosen M, Grilc M, Eschenbacher A, De Meester S, Van Geem KM, Maximizing olefin production via steam cracking of distilled pyrolysis oils from difficult-to-recycle municipal plastic waste and marine litter, Sci Total Environ 2022;838:156092.

[24] Veksha A, Moo JGS, Krikstolaityte V, Oh WD, Chanaka Udayanga WD, Giannis A, Lisak G, Synthesis of $CaCr_2O_4$/carbon nanoplatelets from non-condensable pyrolysis gas of plastics for oxygen reduction reaction and charge storage, J Electroanal Chem 2019;849:113368.

[25] Scheirs J., Overview of commercial pyrolysis processes for waste plastics, in Scheirs J., Kaminsky W. (Eds.), Feedstock recycling and pyrolysis of waste plastics: Converting waste plastics into diesel and other fuels, John Wiley & Sons, Ltd, ISBN: 0-470-02152-7, 2006, pp. 383-433.

[26] Mastral FJ, Esperanza E, Garcia P, Juste M, Pyrolysis of high-density polyethylene in a fluidised bed reactor. Influence of the temperature and residence time, J Anal Appl Pyrolysis 2002:63:1-15.

[27] Abanades A, Ruiz E, Ferruelo EM, Hernandez F, Cabanillas A, Martínez-Val JM, Rubio JA, et al., Experimental analysis of direct thermal methane cracking, Int J. Hydrog Energ 2011;36:12877-12886.

[28] Singh RK, Ruj B, Sadhukhan AK, Gupta P, Thermal degradation of waste plastics under non-sweeping atmosphere: Part 1: Effect of temperature, product optimization, and degradation mechanism, J Environ Manage 2019;239:395-406.

[29] Veksha A, Yin K, Moo JGS, Oh WD, Ahamed A, Chen WQ, Weerachanchai P, Giannis A, Lisak G, Processing of flexible plastic packaging waste into pyrolysis oil and multi-walled carbon nanotubes for electrocatalytic oxygen reduction, J Hazard Mater 2020;387:121256.

[30] Muradov N, Hydrogen via methane decomposition: an application for decarbonization of fossil fuels, Int J Hydrogen Energ 2001;26:1165-1175.

[31] Wu C, Williams PT, Effects of gasification temperature and catalyst ratio on hydrogen production from catalytic steam pyrolysis-gasification of polypropylene. Energy Fuels 2008;22:4125-4132.

[32] Jie X, Li W, Slocombe D et al. Microwave-initiated catalytic deconstruction of plastic waste into hydrogen and high-value carbons. Nat Catal 2020;3:902–912.

[33] Barbarias I, Lopez G, Alvarez J, Artetxe M, Arregi A, Bilbao J, Olazar M., A sequential process for hydrogen production based on continuous HDPE fast pyrolysis and in-line steam reforming, Chem Eng J 2016;296:191-198.

[34] Yeheskel J, Epstein M, Thermolysis of methane in a solar reactor for mass-production of hydrogen and carbon nanomaterials, Carbon 2011;49:4695-4703.

[35] Rodat S, Abanades S, Coulie J, Flamant G, Kinetic modelling of methane decomposition in a tubular solar reactor, Chem Eng J 2009;146:120-127.

[36] Aboul-Enein AA, Awadallah AE, Production of nanostructure carbon materials via non-oxidative thermal degradation of real polypropylene waste plastic using La_2O_3 supported Ni and Ni–Cu catalysts, Polym Degrad Stab 2019;167:157-169.

[37] Veksha A, Chen W, Liang L, Lisak G, Converting polyolefin plastics into few-walled carbon nanotubes via a tandem catalytic process: Importance of gas composition and system configuration, J Hazard Mater 2022;435:128949.

[38] Chen W, Fu X, Veksha A, Lipik V, Lisak G, Few-walled carbon nanotubes derived from shoe waste plastics: Effect of feedstock composition on synthesis, properties and application as CO_2 reduction electrodes, J Clean Prod 2022;356:131868.

[39] Carbon black, Edited by Donnet JB, Bansal RC, Wang MJ, 2nd Ed, 1993:68, ISBN 0-8247-8975-X.

[40] Fan Y, Fowler GD, Zhao M, The past, present and future of carbon black as a rubber reinforcing filler – A review, J Cleaner Prod 2020;247:119115.

[41] Gueret C, Billaud F, Fixari B, Le Perchec P, Thermal coupling of methane, experimental investigations on coke deposits, Carbon 1995;33:159-170.

[42] Geißler T, Abanades A, Heinzel A, Mehravaran K, Müller G, et al., Hydrogen production via methane pyrolysis in a liquid metal bubble column reactor with a packed bed, Chem Eng J 2016;299:192-200.

[43] Alves L, Pereira V, Lagarteira T, Mendes A, Catalytic methane decomposition to boost the energy transition: Scientific and technological advancements, Renewable Sustainable Energy Rev 2021;137:110465.

[44] Robertson CG, Hardman NJ, Nature of carbon black reinforcement of rubber: Perspective on the original polymer nanocomposite, Polymers 2021;13:538.

[45] Dewa K, Ono K, Watanabe A, Takahashi K, Matsukawa Y, Saito Y et al., Evolution of size distribution and morphology of carbon nanoparticles during ethylene pyrolysis, Combustion Flame 2016;163:115-121.

[46] Kiminori Ono, Miki Yanaka, Sho Tanaka, Yasuhiro Saito, Hideyuki Aoki, Okiteru Fukuda, Takayuki Aoki, Togo Yamaguchi, Influence of furnace temperature and residence time on configurations of carbon black, Chem Eng J 2012;200-202:541-548.

[47] Watson AY, Valberg PA, Carbon black and soot: Two different substances, AIHAJ - American Industrial Hygiene Association 2001;62:218-228, DOI: 10.1080/15298660108984625.

[48] Gruber T, Zerda TW, Gerspacher M, Raman studies of heat-treated carbon blacks, Carbon 1994;32:1377-1382.

[49] Quan Y, Liu Q, Zhang S, Zhang S, Comparison of the morphology, chemical composition and microstructure of cryptocrystalline graphite and carbon black, Appl Surf Sci 2018;445:335-341.

[50] Sing KSW, Physisorption of gases by carbon blacks, Carbon 1994;32:1311-1317.

[51] ASTM D1765-16. Standard classification system for carbon blacks used in rubber products.

[52] Okoye CO, Zhu M, Jones I, Zhang J, Zhang Z, Zhang D, An investigation into the preparation of carbon black by partial oxidation of spent tyre pyrolysis oil, Waste Manage 2022;137:110-120.

[53] Ahamed A, Ge L, Zhao K, Veksha A, Bobacka J, Lisak G, Environmental footprint of voltammetric sensors based on screen-printed electrodes: An assessment towards “green” sensor manufacturing, Chemosphere 2021;278:130462.

[54] Latiff NM, Fu X, Mohamed DK, Veksha A, Handayani M, Lisak G, Carbon based copper(II) phthalocyanine catalysts for electrochemical CO_2 reduction: Effect of carbon support on electrocatalytic activity, Carbon 2020;168:245-253.

Graphical abstract